First-Principles Model-based Closed-loop Control of the Current Profile Dynamic Evolution on DIII-D

J.E. Barton 1), M.D. Boyer 1), W. Shi 1), W.P. Wehner 1), E. Schuster 1), T.C. Luce 2), J.R. Ferron 2), M.L. Walker 2), D.A. Humphreys 2), B.G. Penaflor 2) and R.D. Johnson 2)

1) Lehigh University, Bethlehem, Pennsylvania 18015, USA.
2) General Atomics, PO Box 85608, San Diego, California 92186-5608, USA.

e-mail contact of main author: justin.barton@lehigh.edu

Abstract. Recent experiments performed at DIII-D represent the first successful application of first-principles-driven, model-based, closed-loop magnetic profile control in a tokamak. For ITER to be capable of operating in advanced tokamak operating regimes, characterized by a high fusion gain, good plasma confinement, magnetohydrodynamic stability, and a noninductively driven plasma current, for extended periods of time, several challenging plasma control problems still need to be solved. For instance, setting up a suitable toroidal current density profile, which will require active closed-loop profile control, is key for one possible advanced operating scenario characterized by noninductive sustainment of the plasma current and steady-state operation. The current profile evolution in tokamaks is related to the poloidal magnetic flux profile evolution, which is modeled in normalized cylindrical coordinates using a nonlinear partial differential equation referred to as the magnetic diffusion equation. For control design purposes, the magnetic diffusion equation has been combined with empirical correlations obtained from physical observations and experimental data from DIII-D for the electron temperature, plasma resistivity, and noninductive current drive to develop a control-oriented model of the system valid for low confinement mode discharges. This first-principles-driven model was used to synthesize a combined feedforward + feedback control scheme to drive the current profile to a desired target profile. Static and dynamic plasma response models were integrated into the design of the feedback controllers, and as a result, the model-based controllers know in which direction to actuate the system to generate a desired response in the profile evolution thanks to the embedded physics. Therefore, the need for trial-and-error tuning of the control scheme is eliminated, which is desirable for application on ITER where discharges are at a premium. A general framework for real-time feedforward + feedback control of magnetic and kinetic plasma profiles was implemented in the DIII-D Plasma Control System, and experimental results are presented to demonstrate the ability of the first-principles-driven, model-based feedback controllers to control the current profile evolution. These results demonstrate the applicability of this control scheme to active, closed-loop current profile control in advanced operating scenarios on ITER.

1. Introduction

In order for ITER to achieve its scientific objectives, it will need to operate in regimes characterized by a high fusion gain, good confinement, plasma stability, and a noninductively driven plasma current. Two such scenarios are the "hybrid" and "steady-state" advanced scenarios that are characterized by safety factor, or q, profiles with a minimum value higher or equal to one to mitigate plasma instabilities and improve confinement. Thus, active control of $q_{min}(t)$ is desirable. However, to sustain a significant portion of the total plasma current via noninductive means (100% in the case of the "steady-state" scenario), tailoring of the entire q profile is necessary to maximize the bootstrap current and maintain stability. Therefore, techniques to actively control the evolution of the entire q profile during the discharge are of paramount importance to the success of ITER. In this work, we present recent experimental results obtained at DIII-D where first-principles-driven, model-based, closed-loop control of the magnetic profile evolution was successfully demonstrated for the first time in a tokamak.

In this work, we utilize a model-based feedforward + feedback scheme to control the magnetic profile evolution in the tokamak. Embedding the physics of the system into the control design process through a control-oriented dynamic model allows a model-based controller to take into

account the dynamics of the entire q profile in response to the actuators, thus eliminating the need for trial-and-error tuning of the control scheme. In other words, the controller knows in which direction to actuate to generate a desired response in the profile evolution thanks to the embedded physics. Progress towards control-oriented modeling of the current profile evolution has been reported following both data-driven [1, 2] and first-principles-driven [3, 4] approaches.

By following a data-driven modeling approach, linear, dynamic, plasma profile response models were recently obtained from experimental data by performing system identification experiments in JET [1], JT-60U, and DIII-D [2] and were used to design controllers to simultaneously control the magnetic and kinetic plasma profiles. However, as the identified models are linear, they are only valid around the reference plasma state adopted during the system identification experiment. Therefore, the effectiveness of the controllers may be limited when the plasma state moves away from the reference state. Moreover, as these models are device-specific, dedicated system identification experiments are needed in each device, and potentially for each control scenario, to develop model-based controllers. As an alternative to data-driven modeling, first-principles-driven modeling, and subsequent controller design, has the potential of overcoming these limitations. The first-principles-driven model has the advantages of being: (i) adaptable to various machines, (ii) extendable to various equilibrium configurations and operating scenarios, (iii) able to incorporate the nonlinear coupling between the magnetic and kinetic plasma parameters, and (iv) able to explicitly describe the temporal and spatial evolution of the current profile in response to nonlinear control actuation. Therefore, control strategies for various tokamaks operating in different equilibrium configurations can be designed from one model structure.

The poloidal magnetic flux profile evolution, which is modeled by the poloidal magnetic flux diffusion equation, is related to the current profile evolution. The magnetic flux diffusion equation is combined with empirical correlations obtained from physical observations and experimental data from DIII-D for the electron temperature, the plasma resistivity, and the noninductive current drive to obtain a simplified nonlinear, control-oriented, partial differential equation (PDE) model describing the poloidal magnetic flux profile evolution in response to the electric field due to induction, the auxiliary heating and current drive systems (neutral beam injection), and the line average density in low confinement mode discharges [4]. The control-oriented model was integrated into the design of feedback controllers by employing backstepping [5], robust [6], and optimal [7] control theories respectively (see Refs. [8, 9, 10] for a description of these control techniques), and a general framework for real-time feedforward + feedback control of magnetic and kinetic plasma profiles was implemented in the DIII-D Plasma Control System to experimentally test the designed controllers in DIII-D.

2. Current Profile Evolution Model

Any arbitrary quantity that is constant on each magnetic flux surface within the tokamak plasma can be used to index the magnetic flux surfaces. We choose the mean effective minor radius, ρ, of the magnetic flux surface, i.e., $\pi B_{\phi,0}\rho^2 = \Phi$, as the indexing variable, where Φ is the toroidal magnetic flux and $B_{\phi,0}$ is the reference magnetic field at the geometric major radius R_0 of the tokamak. The normalized effective minor radius is defined as $\hat{\rho} = \rho/\rho_b$, where ρ_b is the mean effective minor radius of the last closed magnetic flux surface. The q profile is related to the toroidal current profile in the machine and is defined as $q(\rho,t) = -d\Phi/d\Psi$, where Ψ is the poloidal magnetic flux. By using the constant relationship between ρ and Φ and the definition of $\hat{\rho}$, the safety factor is written as

$$q(\hat{\rho},t) = -\frac{d\Phi}{d\Psi} = -\frac{d\Phi}{2\pi d\psi} = -\frac{B_{\phi,0}\rho_b^2\hat{\rho}}{\partial\psi/\partial\hat{\rho}} \quad , \tag{1}$$

where ψ is the poloidal stream function, which is closely related to the poloidal flux, i.e., $\Psi = 2\pi\psi$. Therefore, we begin by developing a model of the evolution of the poloidal magnetic flux, which is given in normalized cylindrical coordinates by the magnetic diffusion equation [4, 11, 12]

$$\frac{\partial \psi}{\partial t} = \frac{\eta(T_e)}{\mu_0 \rho_b^2 \hat{F}^2} \frac{1}{\hat{\rho}} \frac{\partial}{\partial \hat{\rho}} \left(\hat{\rho} \hat{F} \hat{G} \hat{H} \frac{\partial \psi}{\partial \hat{\rho}} \right) + R_0 \hat{H} \eta(T_e) \frac{\langle \bar{j}_{NI} \cdot \bar{B} \rangle}{B_{\phi,0}} \quad , \tag{2}$$

where t is the time, η is the plasma resistivity, T_e is the electron temperature, μ_0 is the vacuum permeability, $\bar{j}_{NI}$ are the external sources of noninductive current density (neutral beam injection, electron cyclotron heating/current-drive, etc.), $\bar{B}$ is the magnetic field, and $\langle\ \rangle$ denotes a flux-surface average. The parameters $\hat{F}$, $\hat{G}$, and $\hat{H}$ are geometric factors pertaining to the magnetic configuration of a particular plasma equilibrium, and they are given as a function of $\hat{\rho}$ in [4] for a particular magnetic configuration on DIII-D. The boundary conditions are given by

$$\left. \frac{\partial \psi}{\partial \hat{\rho}} \right|_{\hat{\rho}=0} = 0 \qquad , \qquad \left. \frac{\partial \psi}{\partial \hat{\rho}} \right|_{\hat{\rho}=1} = -\frac{\mu_0}{2\pi} \frac{R_0}{\hat{G}\Big|_{\hat{\rho}=1} \hat{H}\Big|_{\hat{\rho}=1}} I(t) \quad , \tag{3}$$

where $I(t)$ denotes the total plasma current.

The magnetic diffusion equation (2) is closed by combining it with empirical correlations obtained from physical observations and experimental data from DIII-D for the electron temperature, the plasma resistivity, and the noninductive current drive during low confinement mode discharges [4]. The q profile (1) is inversely dependent on the gradient of the poloidal stream function $\partial\psi/\partial\hat{\rho}$, therefore, it is chosen to be the controlled variable and is denoted by

$$\theta(\hat{\rho}, t) \equiv \partial\psi/\partial\hat{\rho}(\hat{\rho}, t) \quad . \tag{4}$$

After some mathematical manipulations, the first-principles-driven, control-oriented, PDE governing the evolution of $\theta(\hat{\rho}, t)$ is found to be

$$\frac{\partial \theta}{\partial t} = \left[h_0(\hat{\rho}) \frac{\partial^2 \theta}{\partial \hat{\rho}^2} + h_1(\hat{\rho}) \frac{\partial \theta}{\partial \hat{\rho}} + h_2(\hat{\rho}) \theta \right] u_1(t) + h_3(\hat{\rho}) u_2(t) \quad , \tag{5}$$

with boundary conditions

$$\theta(0, t) = 0 \qquad , \qquad \theta(1, t) = -k_3 u_3(t) \quad , \tag{6}$$

where $h_0(\hat{\rho})$, $h_1(\hat{\rho})$, $h_2(\hat{\rho})$, and $h_3(\hat{\rho})$ are functions of the empirical models, k_3 is a constant, and

$$u_1(t) = \left(\frac{\bar{n}(t)}{I(t)\sqrt{P_{tot}(t)}} \right)^{3/2} \qquad u_2(t) = \frac{\sqrt{P_{tot}(t)}}{I(t)} \qquad u_3(t) = I(t) \tag{7}$$

are the diffusivity, interior, and boundary control actuators respectively, where $P_{tot}(t)$ is the total average neutral beam power injected into the plasma and $\bar{n}(t)$ is the line average density [5, 6, 7]. This first-principles-driven model contains the physics information of how the dynamics of the poloidal flux gradient profile are influenced by the control actuators. The goal is to convert the physics information contained in the model into a form suitable to synthesize a feedback controller, thus allowing the physics described by the model to be embedded into the feedback controller. We addressed this design challenge by employing backstepping [5], robust [6], and optimal [7] control theories respectively, and we now discuss the synthesis of the algorithms.

3. Overview of Feedback Control Synthesis

The strategy we employ to control the magnetic profile evolution is a feedforward + feedback control scheme. The feedforward component is computed off-line and is designed to obtain the best possible magnetic-profile/target-profile matching based on the evolution of the system predicted by the control-oriented model. To add robustness to the control scheme, the feedback component is computed on-line and is designed to track a desired target trajectory, reject external disturbances, and account for the uncertainties in the model used for the control design. Unique characteristics of the model-based control approach are: (i) the use of first-principles-driven models for the control synthesis, (ii) the integration of both static and dynamic models into the design of the feedback controllers, and (iii) nonlinear control actuation.

A Backstepping controller

The backstepping theory [8] is well suited for control problems where the system can be actuated at the boundary of the spatial domain. In Ref. [5], we exploit the strong influence of the boundary control input on the system (5) and seek a boundary feedback control law by employing the backstepping technique, i.e., $u_1(t) = u_{1_{FF}}(t)$, $u_2(t) = u_{2_{FF}}(t)$, and $u_3(t) = u_{3_{FF}}(t) + u_{3_{FB}}(t)$, where $(\cdot)_{FF}$ denotes a feedforward quantity and $(\cdot)_{FB}$ denotes a feedback quantity. In order to facilitate the synthesis of the boundary feedback control law, the governing infinite dimensional PDE (5) is discretized in space by employing a truncated Taylor series expansion to approximate the spatial derivatives to obtain a finite dimensional system of ordinary differential equations (ODEs). A backstepping transformation is then sought to transform the reduced-order model into an asymptotically stable target system. A stabilizing boundary feedback control law is then obtained by evaluating this transformation at $\hat{\rho} = 1$. Finally, by employing the inverse nonlinear transformations resulting from (7), we obtain closed-loop trajectories for $I(t)$, $P_{tot}(t)$, and $\bar{n}(t)$.

B Robust and optimal controllers

In Refs. [6, 7], we employ robust [9] and optimal [10] control theories to synthesize feedback control laws that utilize all of the control actuators (diffusivity, interior, and boundary). We once again approximate the governing PDE (5) by a finite dimensional system of ODE's by employing a truncated Taylor series expansion in space. While the state of the reduced-order model is linearized around a given feedforward trajectory, the control input nonlinearities are preserved through the nonlinear transformations (7) to obtain a time-varying state-space representation of the deviation dynamics. As we only have three inputs, we can only independently control three linear combinations of the output of the system. Therefore, we determine the preferred input/output directions of the system by employing a singular value decomposition of the static gain matrix of the system model. In Ref. [6], the time-varying state-space system is represented as a nominal time-invariant model plus a bounded uncertain component, which is combined with the preferred input/output directions to design a robust feedback controller that guarantees the closed-loop system remains stable in the presence of the uncertainty. In Ref. [7], the time-varying state-space system is combined with the preferred input/output directions to design a linear-quadratic-integral controller. Incorporating the preferred input/output directions into the control synthesis ensures the controllers will not actuate the system with an excessive amount of control energy in a direction it does not easily respond to. Finally, by using the inverse nonlinear transformations resulting from (7), we obtain closed-loop trajectories for $I(t)$, $P_{tot}(t)$, and $\bar{n}(t)$.

4. Experimental Testing of Control Algorithms in Low Confinement Discharges

Based on the physical design of the DIII-D tokamak, the nonlinear dynamics of the plasma, and the magnitude and rate of change constraints of the actuators, there are a limited number of target poloidal flux gradient profiles that are physically achievable by the machine for a given initial θ profile no matter what type of profile control strategy is employed. Therefore, the experimental goals were to determine the ability of the feedback controllers synthesized from a first-principles-driven model of the poloidal flux profile evolution to drive the system to a target profile that was (i) a priori known to be physically achievable by the machine or (ii) a priori not known to be physically achievable by the machine. Towards this goal, we first sought a target poloidal flux gradient profile evolution that was physically achievable by the machine. This was accomplished by executing a feedfoward-control-only discharge with a nominal set of feedforward control inputs in shot #145477 (Fig. 1). From this discharge we extracted a physically achievable target profile evolution that was employed to test the feedback controllers in reference tracking and disturbance rejections experiments. It is important to note that the requests made by the combined feedforward + feedback controller are the references to the respective control loops commanding the physical actuators.

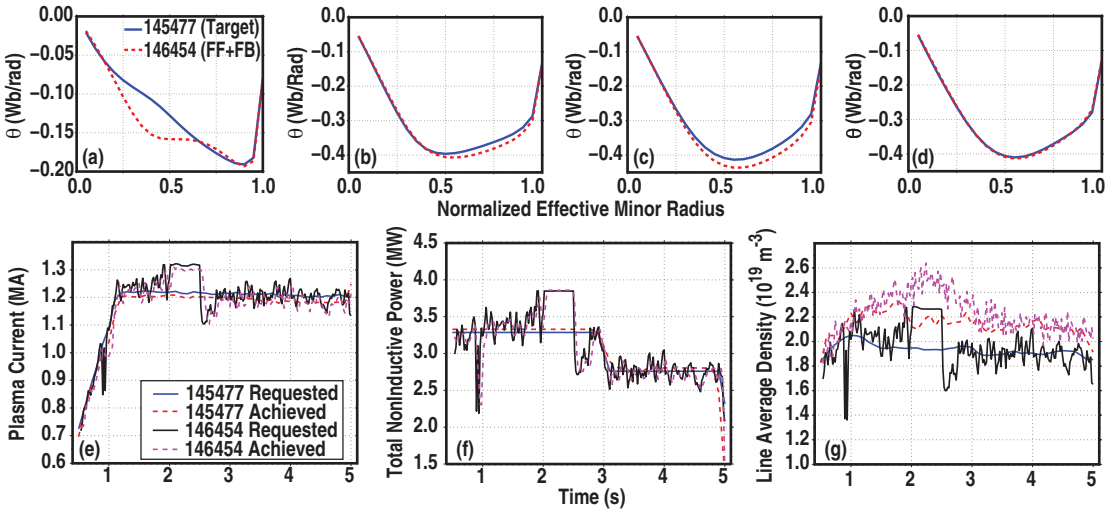

FIG. 1. Illustration of backstepping feedback controller's performance. Poloidal flux gradient $\theta(\hat{\rho})$ at time: (a) $t = 0.538$ s, (b) $t = 1.998$ s, (c) $t = 2.498$ s, and (d) $t = 4.318$ s, and control trajectory comparison: (e) plasma current (MA), (f) total noninductive power (MW), and (g) line average density (10^{19} m^{-3}). Shot #146454 was feedforward + feedback controlled in the presence of an input disturbance, and shot #145477 was feedforward controlled and employed to obtain a physically achievable target profile evolution.

A Backstepping feedback control results

In this subsection, we present the results of a test designed to determine the ability of the backstepping feedback controller [5] to reject input disturbances and perturbed initial conditions. In shot #146454, the profile evolution extracted from shot #145477 was employed as the target profile evolution and an input disturbance of 0.1 MA was added to the nominal feedforward control input u_3 during the time interval $t = [0.5, 2.5]$ s. The feedback controller was turned on during the time interval $t = [0.5, 2.0]$ s to test the disturbance rejection capabilities of the controller and was switched off during the time interval $t = [2.0, 2.5]$ s to observe the influence of the input disturbance on the θ profile without the presence of feedback control. Finally, at $t = 2.5$ s, the feedback controller was turned on for the remainder of the discharge and the input disturbance was removed to determine if the feedback controller could recover the target profile despite the error caused by the uncontrolled drift.

In Figs. 1(a-d), the θ profiles achieved during the feedforward + feedback, disturbed shot #146454 are compared with the desired profiles achieved during the target discharge at several times. Figure 1(a) shows the discrepancy between the initial condition of the target and feedforward + feedback shot. Shortly before the feedback controller was turned off at $t = 2.0$ s, it was able to mostly (i) overcome the initial condition error and (ii) reject the artificially applied input disturbance and achieve a profile close to the desired one as shown in Fig. 1(b). Figure 1(c) shows the increased error resulting from the disturbance after the uncontrolled drift phase (time interval $t = [2.0, 2.5]$ s), while Fig. 1(d) depicts the successful recovery of the desired profile after the controller was turned back on and the artificial disturbance was removed. Finally, the actuator requests and achieved values are compared in Figs. 1(e-g). It should be noted that while the total plasma current and total average neutral beam power are tightly controlled and the requests were reproduced quite well by the physical control loops, the request for line averaged density was not achieved. This represented an additional input disturbance, and the controller appears to be robust to the loose control of the density.

B Robust feedback control results

In this subsection, we present the results of a test designed to determine the reference tracking capabilities of the robust feedback controller [6] in the DIII-D tokamak during the ramp-up and early flattop phases of the discharge. A feedfoward-control-only discharge was executed in shot

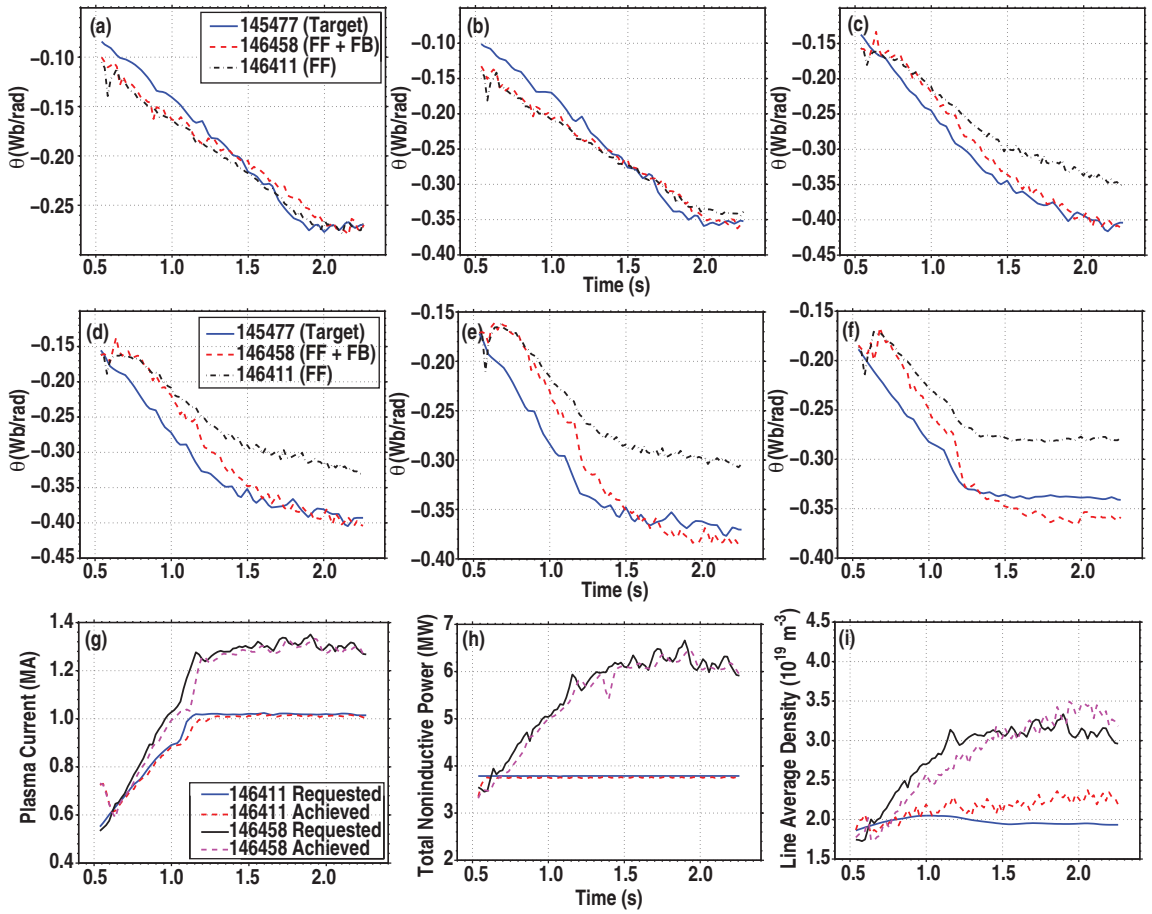

FIG. 2. Illustration of robust feedback controller's performance. Time trace of poloidal flux gradient θ at normalized radii: (a) $\hat{\rho} = 0.3$, (b) $\hat{\rho} = 0.4$, (c) $\hat{\rho} = 0.6$, (d) $\hat{\rho} = 0.7$, (e) $\hat{\rho} = 0.8$, and (f) $\hat{\rho} = 0.9$ and control trajectory comparison: (g) plasma current (MA), (h) total noninductive power (MW), and (i) line average density (10^{19} m^{-3}).

#146411, and a feedforward + feedback control discharge was executed in shot #146458 to determine the ability of the feedback controller to track the target profile evolution, which was chosen as the profile evolution extracted from shot #145477. During the feedforward + feedback control discharge, the feedback controller was active for the duration of the experiment, and the feedforward control inputs from shot #146411 were used.

Time traces of the poloidal flux gradient θ achieved during the target discharge, the feedforward + feedback control discharge, and the feedforward control discharge are shown in Figs. 2(a-f) at several normalized radii. As shown in the figures, the target profile evolution was not achieved by employing only feedforward control, therefore, feedback control is necessary to attempt to drive the system to the target evolution. The feedback controller can actuate the θ profile evolution through diffusivity, interior, and boundary control. As the boundary control is one of the more influential actuators, the feedback controller can more effectively control the θ profile near the plasma boundary. As a result, a tracking error in the interior of the plasma will take longer to eliminate because the control actuation applied at the plasma boundary will have to diffuse towards the center of the plasma. This behavior is exemplified in the time traces of θ at normalized radii $\hat{\rho} = 0.6$, 0.7, 0.8, and 0.9. The θ evolution at $\hat{\rho} = 0.6$ and 0.7 was initially below the desired target evolution during the feedforward + feedback control discharge. As a result, the feedback controller caused θ at $\hat{\rho} = 0.8$ and 0.9 to overshoot the desired target evolution in order to cause the θ evolution at $\hat{\rho} = 0.6$ and 0.7 to increase towards the target evolution through resistive diffusion. Once the target θ evolution was achieved at $\hat{\rho} = 0.6$ and 0.7 at the time $t = 2.0$ s, the feedback controller began to reduce the tracking error at the normalized radii $\hat{\rho} = 0.8$ and 0.9 during the time interval $t = [2.0, 2.25]$ s. A comparison of the

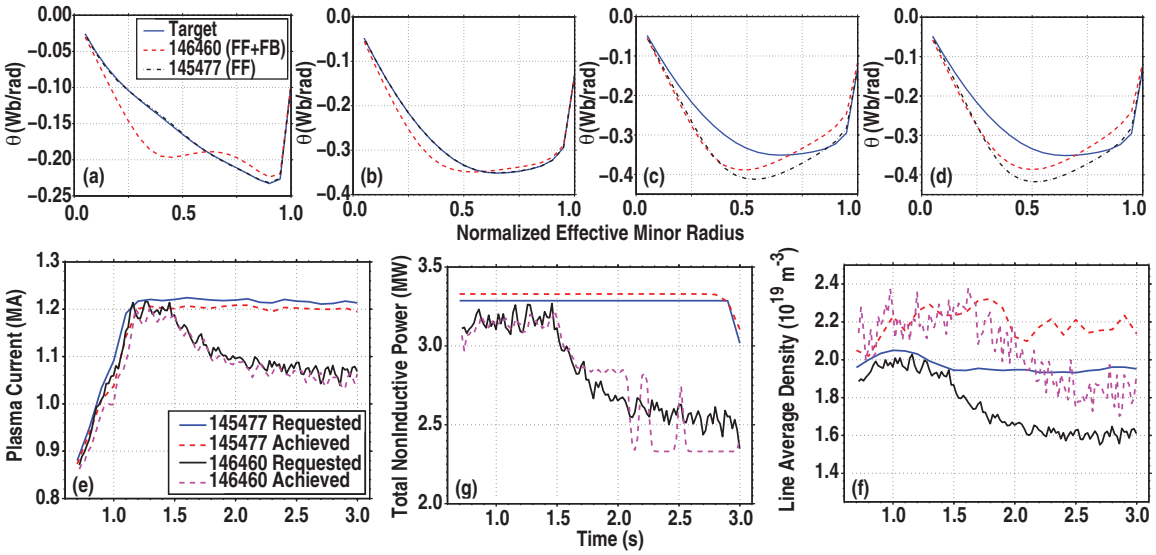

FIG. 3. Illustration of optimal feedback controller's performance. Poloidal flux gradient $\theta(\hat{\rho})$ at time: (a) $t = 0.718\,s$, (b) $t = 1.498\,s$, (c) $t = 2.398\,s$, and (d) $t = 2.998\,s$, and control trajectory comparison: (e) plasma current (MA), (f) total noninductive power (MW), and (g) line average density ($10^{19}\,m^{-3}$).

actuator trajectories during the feedforward and feedforward + feedback control discharges is shown in Figs. 2(g-i). The feedback component of the combined controller modified the actuator trajectories throughout the feedforward + feedback control discharge in order to (i) overcome the initial condition error and (ii) track the target profile evolution. Also shown in the figures is the ability of the control loops commanding the physical actuators to follow the requests made by the control algorithm. The control loops commanding the total plasma current and the total average neutral beam power were able to follow the requests very well, and the control loop commanding the line average density was able to follow the request reasonably well.

C Optimal feedback control results

In the previous subsections, the profile evolution of a feedforward-control-only discharge was used as the target profile evolution for the feedforward + feedback shots. This guaranteed the target was an achievable θ profile evolution. In this subsection, we again use the profile evolution of a feedforward-control-only discharge as the target, however, for a short time interval, we hold the target profile constant rather than allowing it to evolve as it did in feedforward. By freezing the target, we task the feedback controller with trying to drive the system to evolve in a manner not observed in any feedforward control experiments. Therefore, this target profile evolution may not even be achievable given input saturation limits and the fact that the system is underactuated. As a result, this is a much more challenging reference tracking problem. The optimal feedback controller [7], which was successfully tested in both disturbance rejection and reference tracking scenarios previously, was used for this experiment. In shot #146460, the target profile evolution was chosen as the profile evolution achieved during shot #145477 except that the target profile was frozen at $t = 1.5\,s$ and held constant until $t = 3.0\,s$, i.e., the profile achieved in shot #145477 at the time $t = 1.5\,s$ was used as the target profile during the time interval $t = [1.5, 3.0]\,s$. In shot #146460, the feedback controller was active for the duration of the experiment.

In Figs. 3(a-d), the poloidal flux gradient θ profiles achieved during the feedforward + feedback and feedforward control discharges are compared with the desired target profiles at several times. Figure 3(a) shows the discrepancy between the initial condition of the target and the feedforward + feedback shot, while Fig. 3(b) shows how the controller has progressed toward achieving the desired profile evolution after a short time. Figures 3(c-d) depict the profile tracking results during the "frozen target" time interval in which the target profile was not necessarily physically achievable. The feedback controller pushed the θ profile away from the feedforward

profile evolution and towards the specified target, but the tracking results do not improve significantly between the two time instances shown. This behavior occurred because the controller is designed to determine and only attempt to track the physically achievable component of the target profile as predicted by the model. This design choice prevents the controller from using an excessive amount of actuator effort in an attempt to track the unachievable components of the target. Based on the actuator requests and achieved values, which are compared in Figs. 3(e-g), it is apparent that by $t = 3.0\,\mathrm{s}$ the controller essentially reached a steady set of inputs, which indicates it has successfully driven the system to the predicted achievable target profile.

5. Conclusions and Future Work

For the first time in a tokamak, first-principles-driven, model-based, closed-loop control of the magnetic profile evolution was demonstrated in DIII-D by employing robust, optimal, and backstepping control theories. Now that the performance of the synthesized feedback controllers has been experimentally validated in L-mode, the combined feedforward + feedback control scheme will be extended to H-mode advanced tokamak operating scenarios. Towards this goal, the poloidal flux diffusion equation will be combined with empirical models obtained from physical observations and experimental data for the electron density and temperature profiles, plasma resistivity, and noninductive current drives (including the effects of the bootstrap current, which were neglected in L-mode) to obtain a simplified nonlinear, control-oriented PDE model of the poloidal flux profile and stored energy evolutions valid for H-mode discharges. Alternatively, the empirical electron temperature model could be replaced by the electron heat transport equation, which would be combined with empirical models of the electron heat conductivity and heat sources, to obtain a simplified nonlinear, control-oriented PDE model of the poloidal flux and electron temperature profile evolutions. The heating and current drive actuators, i.e., electron cyclotron heating/current-drive, ion cyclotron heating, and neutral beam heating/current-drive, will be modeled individually rather than together, which may improve the controllability of the current profile by providing additional independent actuators. By employing these first-principles-driven models, control schemes will be proposed to regulate both the magnetic and kinetic plasma profiles around desired target profiles simultaneously in H-mode discharges.

This work was supported by the NSF CAREER award program (ECCS-0645086) and the U.S. Department of Energy (DE-FG02-09ER55064, DE-FG02-92ER54141 and DE-FC02-04ER54698).

References

[1] MOREAU, D., et al., Nucl. Fusion **48** (2008) 106001.
[2] MOREAU, D., et al., Nucl. Fusion **51** (2011) 063009.
[3] WITRANT, E., et al., Plasma Phys. Controlled Fusion **49** (2007) 1075.
[4] OU, Y., et al., Fusion Eng. and Design **82** (2007) 1153.
[5] BOYER, M.D., et al., Backstepping Control of the Plasma Current Profile in the DIII-D Tokamak, in *American Control Conference*, pp. 2996–3001 (2012).
[6] BARTON, J.E., et al., First-Principles Model-Based Robust Control of the Current Evolution in the DIII-D Tokamak, in *American Control Conference*, pp. 2134–2140 (2012).
[7] BOYER, M.D., et al., Current Profile Tracking for the DIII-D Tokamak via LQI Optimal Control, in *Proc. of 51st IEEE Conference on Decision and Control* (2012).
[8] KHALIL, H., *Nonlinear Systems Third Edition*, Prentice Hall, New Jersey, USA (2002).
[9] SKOGESTAD, S. and POSTLETHWAITE, I., *Multivariable Feedback Control: Analysis and Design Second Edition*, John Wiley & Sons, West Sussex, England (2005).
[10] NAIDU, D., *Optimal Control Systems*, CRC Press, Florida, USA (2003).
[11] HINTON, F.L. and HAZELTINE, R.D., Reviews of Modern Physics **48** (1976) 239.
[12] BLUM, J., *Numerical Simulation and Optimal Control in Plasma Physics: With Applications to Tokamaks*, John Wiley & Sons, Paris (1989).